Development of a Control System for the Tennessee Eastman Control Problem that Eliminates Excessive Variability in Control Actions

Stopakevych A. O., Stopakevych O. A.,

Odesa Polytechnic National University
Odesa, Ukraine

Abstract. The Tennessee-Eastman Process (TEP) model has served as a globally recognized standard for evaluating advanced control methods for unstable technological processes for over 20 years. Research data published in leading scientific journals are used to evaluate modern control algorithms and are accumulated in a dedicated repository. Analysis shows that the problem of eliminating unwanted oscillations in control actions caused by measurement noise and sensor discreteness, without reducing robustness and cost-effectiveness, remains unresolved. To achieve this goal, the following tasks were solved: a multi-faceted analysis of the physical, dynamic, and economic characteristics of the process was performed, based on which a hierarchical control structure with decentralized PI controllers was synthesized; advanced filtering methods have been developed and implemented, including discrete Kalman filters with constant-rate models for reconstructing continuous concentration signals, second-order setpoint filters in cascaded loops, and Smith predictors for delay compensation. Cross-coupling compensation and pressure stabilization schemes using additional control channels have been proposed. The most important results include the virtually complete suppression of high-frequency noise from level, flow, and concentration sensors without introducing critical phase delays; the elimination of excessive oscillations in valves and pumps, which radically reduces their mechanical wear; and the successful compensation of typical process disturbances while maintaining process operability. The significance of the obtained results lies in the fact that the proposed approach demonstrates for the first time the possibility of integrating observers and filters into a classical circuit architecture for controlling an unstable chemical engineering process.

Keywords: automatic control system, technologically unstable process, Tennessee Eastman control problem, measurement noise, hierarchical control structure, Kalman filter, Smith predictor, cross-links.

DOI: https://doi.org/10.52254/1857-0070.2026.4-72.10
UDC: 681.51

Dezvoltarea unui sistem de control pentru Problema de Control Eastman din Tennessee care elimină variabilitatea excesivă a acțiunilor de control

Stopakevyci A.O., Stopakevyci O.A.
Universitatea Națională Politehnică din Odesa, Odesa, Ucraina

Rezumat. Modelul procesului Tennessee Eastman (Tennessee Eastman Process – TEP) reprezintă de peste 20 de ani un etalon recunoscut la nivel internațional pentru evaluarea metodelor avansate de control al proceselor tehnologice instabile. Analiza efectuată evidențiază faptul că eliminarea oscilațiilor nedorite ale semnalelor de comandă, provocate de zgomotul de măsurare și de discretizarea semnalelor furnizate de senzori, fără diminuarea robusteții sistemului și a eficienței economice, rămâne o problemă nerezolvată. Pentru atingerea acestui obiectiv, au fost realizate următoarele activități: analiza multidimensională a caracteristicilor fizice, dinamice și economice ale procesului, în vederea sintetizării unei structuri ierarhice de control bazate pe regulatoare PI descentralizate; dezvoltarea și implementarea unor metode avansate de filtrare, inclusiv a filtrelor Kalman discrete bazate pe modele cu rată constantă, pentru estimarea semnalelor continue de concentrație, a filtrelor de ordinul al doilea pentru filtrarea valorilor de referință în buclele de reglare în cascadă și a predictorilor Smith pentru compensarea întârzierilor; precum și elaborarea unor scheme de compensare a cuplajelor dintre buclele de reglare și de stabilizare a presiunii prin utilizarea unor canale suplimentare de comandă. Principalele rezultate obținute includ atenuarea aproape completă a zgomotului de înaltă frecvență provenit de la senzorii de nivel, debit și concentrație, fără introducerea unor întârzieri de fază semnificative; reducerea oscilațiilor excesive ale elementelor de execuție, precum valvele și pompele, contribuind astfel la diminuarea uzurii mecanice; și compensarea eficientă a perturbațiilor caracteristice procesului, cu menținerea stabilității și a capacității de funcționare a acestuia. Importanța rezultatelor constă în demonstrarea posibilității de integrare a observatoarelor și a filtrelor într-o arhitectură clasică de control în buclă, aplicată unui proces instabil din industria chimică.

© Stopakevych A. O., Stopakevych O. A., 2026

Cuvinte-cheie: sistem de control automat, proces instabil tehnologic, problema de control Tennessee Eastman, zgomot de măsurare, structură ierarhică de control, filtru Kalman, predictor Smith, legături încrucișate.

Разработка системы управления для Tennesee Eastman Control Problem в которой отсутствует чрезмерная колебательность управляющих воздействий

Стопакевич А. Ал., Стопакевич Ал. А.
Национальный университет «Одесская политехника», Одесса, Украина

***Аннотация*.** Признанным в мире стандартом для оценки передовых методов управления неустойчивыми технологическими процессами уже в течение более 20 лет служит модель процесса Теннесси-Истман (TEP). Данные, полученные в результате исследований, опубликованные в ведущих научных журналах, используются для оценки современных алгоритмов управления и накапливаются в специальном репозитории. Анализ показывает, что задача устранения нежелательной колебательности управляющих воздействий, обусловленной шумами измерений и дискретностью датчиков, без снижения робастности и экономической эффективности, до сих пор не решена. Для достижения поставленной цели решены следующие задачи: выполнен многоаспектный анализ физических, динамических и экономических особенностей процесса, на основе которого синтезирована иерархическая структура управления с децентрализованными ПИ-регуляторами; разработаны и разработаны методы продвинутой фильтрации, включая дискретные фильтры Калмана с моделями постоянной скорости для восстановления непрерывных сигналов концентраций, фильтры заданий второго порядка в каскадных контурах и предикторы Смита для компенсации запаздываний; предложены схемы компенсации перекрестных связей и стабилизации давления с использованием дополнительных управляющих каналов. Наиболее важными результатами являются практически полное подавление влияния высокочастотных шумов датчиков уровня, расхода и концентрации без внесения критического фазового запаздывания, устранение излишней колебательности клапанов и насосов, что радикально снижает их механический износ, а также успешная компенсация типовых технологических возмущений с сохранением работоспособности процесса. Значимость полученных результатов состоит в том, что предложенный подход впервые демонстрирует возможность интеграции наблюдателей и фильтров в классическую схемотехническую архитектуру управления неустойчивым химико-технологическим процессом, что позволяет достичь высокого качества регулирования и снизить среднюю себестоимость производства, избегая при этом недостатков «черного ящика», свойственных многомерным системам класса MPC, и обеспечивая практическую применимость в промышленных условиях.

***Ключевые слова*:** система автоматического управления, технологически неустойчивый процесс, Задача управления Tennessee Eastman, шумы измерений, иерархическая структура управления, фильтр Калмана, предиктор Смита, перекрестные связи.

1 INTRODUCTION

Researches in process control often neglects the influence of measuring equipment and actuators on closed-loop control performance. While this simplification is generally acceptable for open-loop stable processes, ignoring equipment operation for open-loop unstable processes can lead to modeling errors.

This article addresses this gap through the benchmark of the Tennessee Eastman Control Problem (TECP), a classic problem in process automation.

To improve the energy efficiency of distillation in the Tennessee Eastman process (TEP), special structural solutions are used that generate strong nonlinearity, process instability, and significant cross-couplings in control channels.

The simulator for this energy-intensive, unstable process with recirculation [1–4] includes modeling of equipment effects that significantly affect the performance of the closed-loop control system. Thus, the TEP simulator is a suitable tool for comprehensive studies applied to complex, inherently unstable, energy-intensive industrial processes.

2 ANALYSIS OF THE TECP

2.1 The plant as a control object

TEP is a classic benchmark for control system analysis [5], first described in [6]. Its key feature is that the process is open-loop unstable due to multiple input and recirculation flows, parallel reactions, and nonlinear mass and energy balances. The model was implemented using software code that cannot be reduced to simple equations. Without control, a plant shutdown occurs within an hour, and with disturbances, within minutes. TEP control requires comprehensive maintenance of material and energy balance, taking into account strict safety and economic constraints.

The general diagram of TEP is shown in Fig.1.

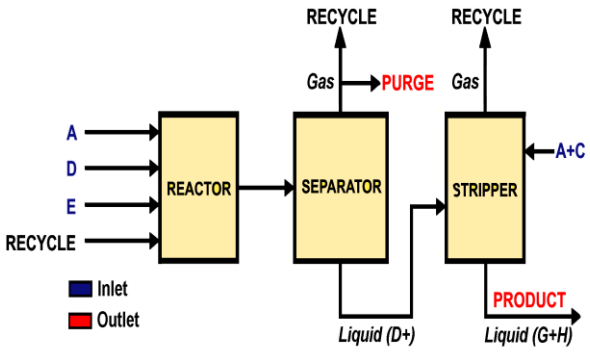


Fig.1. Principal diagram of TEP.

The process model is based on the following assumptions:
1) There are 8 components: *A, B, C, D, E, F, G, H*.
2) Mixings in all vessels are ideal.
3) *A, B, C* do not condense.
4) *B* is an inert gas that requires removal.
5) All gases behave as ideal gases.
6) The equilibrium is subject to Raoult's law.
7) The pressures of *D-H* are determined by the Antoine equation.

The key vessel in the process is a reactor. The main chemical reactions are as follows:

$$A_{(g)} + C_{(g)} + D_{(g)} \rightarrow G_{(l)},\ A_{(g)} + C_{(g)} + E_{(g)} \rightarrow H_{(l)},$$
$$\frac{1}{3}\cdot A_{(g)} + D_{(g)} + \frac{1}{3}\cdot E_{(g)} \rightarrow F_{(l)} \quad (1)$$

where the index l denotes the liquid phase, and the index g denotes the gas phase.

Reactor heat is removed by water cooling. Gaseous products exit to a condenser and separator, while uncondensed components are recycled. Impurity *B* is purged, affecting *A*'s pressure and the *A*/*B* ratio (4–6 hour equilibrium). TEP's instability is driven by temperature and pressure: increasing either the temperature or the purge rate accelerates reactions, consequently decreasing system pressure.

Two versions of the mathematical balance equations [7] include 19 variables. First-order gas-phase reactions obey the Arrhenius law, depending on temperature, partial pressures, and vapor volume. The stirrer affects only heat transfer.

2.2 Control system objectives

The control problem encompasses four primary objectives: 1) enforce physical process constraints; 2) ensure a specified production rate and product composition; 3) ensure operability under a specified set of disturbances associated with changes in composition, feed temperature, reaction rate drift in the reactor, actuator failures or valve stiction; 4) maximize profit: revenue minus operating costs.

2.3 General overview of the control problem

The process is open-loop unstable. To achieve baseline operability, levels in the separator and stripper must be stabilized. Creating an adequate linear multivariable model is impossible due to strong nonlinearity (e.g. exponential temperature dependence described by the Arrhenius equation). Cross-couplings have complex dynamics with time delays, and the linearized model (the Jacobian matrix) loses validity with a temperature change of just 2–3°C. Control is further complicated by non-Gaussian noise, drifts, and equipment malfunctions.

2.4 Classical model analysis

The original TEP simulator was written in FORTRAN [6], and similar code is available in [8]. Arguably, the most practical implementation of the simulator is in C as a MEX module for MATLAB [9]: it is characterized by high speed, compatibility with Simulink solvers, and a configurable random number generator for reproducibility. The recent Simulink-based simulator [10] is computationally heavier than [9].

In [11–13], continuous-time (CM, 38 eigenvalues) and discrete-time (DM, 32 eigenvalues) linearized models in MATLAB were studied based on the simulator [9]. CM captures resonance phenomena that are absent in DM. The system is input-controllable and observable, but not output-controllable; non-minimum-phase dynamics are absent. A high condition number (CN) indicates strong cross-coupling and hypersensitivity to input changes, which causes computational artifacts. Due to the presence of discrete measurements, "direct" linearization does not provide an adequate control model.

In [14], the model is split into stable and unstable parts (linked to vessel levels). To avoid a steam-induced RHP zero, reactor temperature is controlled instead. The poles are stabilized using separator liquid, product, and cooling water flows.

The coupling analysis in [16] was performed using the REGA method based on a 12x12 FOPDT matrix. The method identified three strongly coupled groups of variables, confirming the strong cross-couplings between temperature, pressure, and levels in the main vessels.

2.5 Approaches to plantwide control structure selection

We identified three main universal approaches to systematically solving the problem of constructing a plant-wide control system, which have been applied to TEP.

Approach #1. Material balance stabilization prevents recirculation "snowballing" [15, 7]. Levels are regulated via the Buckley approach [16, 17] and pressure via *A+C* flow. Luyben's P-controller scheme [18] handles disturbances but suffers from noise sensitivity, which can be mitigated by SMC controllers [19].

Approach #2. Self-optimization (SOC) [20] maintains variables at active constraints to minimize compressor load and achieve economic optimums [21]. Existing PI-based schemes exhibit delayed pressure control and high cross-coupling, leading to further theoretical developments [22] and modified mode-switching strategies [23].

Approach #3. Thermodynamic [24] minimizes entropy across a mass/energy network, transforming the stripper into a rectifier [25]. It relies heavily on steady-state behavior, necessitating complex PI tuning optimization [26] to compensate for neglected dynamics.

Common feature: All approaches use steady-state models for initial synthesis, providing a solid starting point despite imperfect transient responses.

2.6 Optimal steady-state mode

The optimal mode maintains profitability, which is defined as the product revenue minus operating costs. The method for calculating operating costs is given in [6]. Total operating costs are the sum of: 1) cost of waste (purge) × Purge flow rate; 2) cost of impurity losses × Product flow rate; 3) cost of compressor operation × Energy consumed; 4) cost of steam × Steam consumption. The nominal cost is 170.6 /hour.

Ricker [27–29] first systematically studied the TEP's economic optimum. While lacking a general methodology, his four proposed modes became standard. A major drawback of steady-state optimization is the risk of dynamic instability during disturbances. Ricker detuned PI controllers for stability. Later, his scheme was improved using static decoupling [30] and a Fuzzy-PI controller [31] for better product composition stabilization.

2.7 Two-level schemes with MPC

Ricker showed that MPC (e.g., NMPC) offers no significant advantages for the TEP due to conflicting objectives [28]. While Siemens claimed MPC benefits [32], their tests used a simplified empirical model rather than the rigorous simulator, highlighting that classical MPC lacks robustness for unstable plants. Recently, [33] evaluated three non-classical MPC variants, achieving positive results only with a two-phase MPC. This required an empirically modified dynamic model incorporating squared flow rates and an independent reactor temperature controller. However, this approach has drawbacks: the 0.2-hour control interval risks destabilizing the process, and the underlying linear model remains inaccurate. Ultimately, the success relied heavily on empirical workarounds, such as introducing non-essential variables and weakening the Kalman filter, rather than robust modeling

2.8 Channel-oriented analysis of process dynamics with speed evaluation

The process time scale is one hour, with transients lasting from hours to days. Control loops are classified by speed: fast (flow, temperature, pressure), medium (concentration), and slow (levels). High noise in level and flow sensors causes actuator oscillations, whereas pressure and temperature sensors have low noise. Concentration sensors feature 0.1–0.25 hour sampling and dead times. Because material balances destabilize quickly, disturbance rejection must rely on indirect parameters.

Although the plant has 41 measured and 12 manipulated variables, relying on [21] reduces the active controls to 9 by excluding u_5 and u_9, and fixing u_{12}. Correlation [11, 12] and decomposition [34] analyses are visualized in Fig. 2.

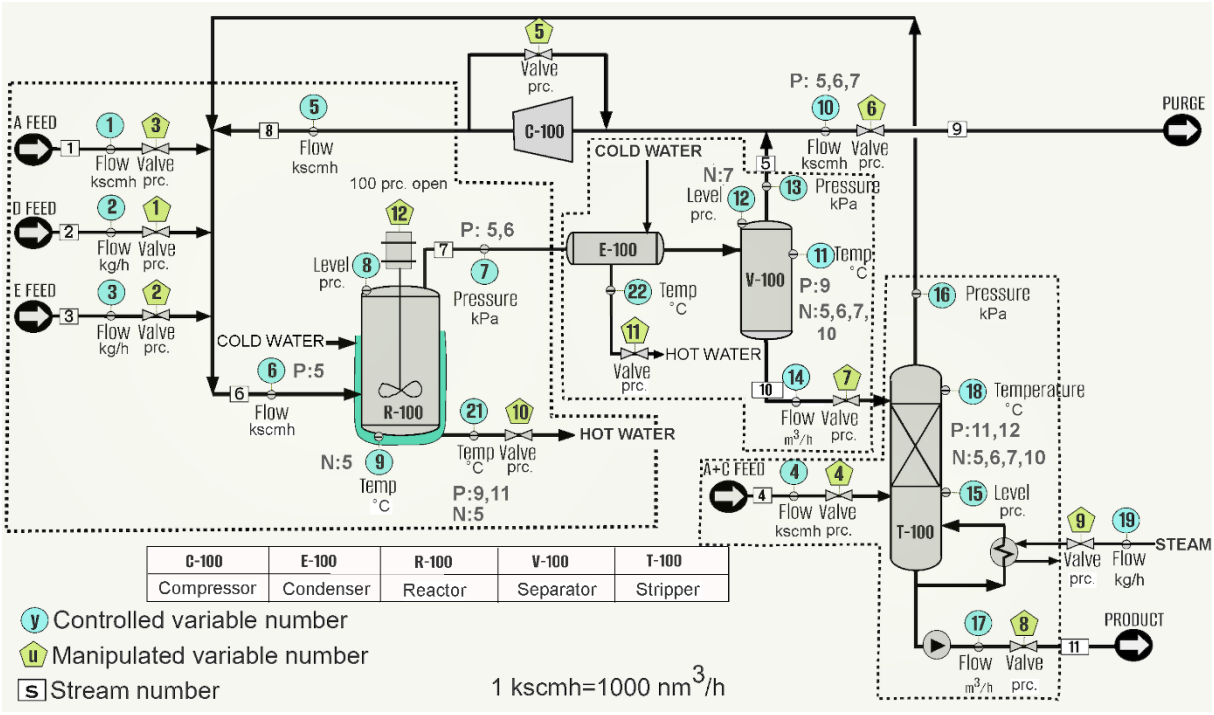
2.9 Multi-level process control

The control problem involves three hierarchical objectives: safety, maintaining reactant ratios, and minimizing operating costs. Transferring these to an MPC reduces flexibility because it relies on an inaccurate model and acts as a non-transparent "black box" with high reconfiguration times. Unlike MPC, a decentralized multi-loop architecture allows engineers to quickly localize and correct problems, making it advisable for multilevel TEP control.

3 PROBLEM STATEMENT

Our analysis shows that a hierarchical control system is optimal. Its base level is built on single-loop (SISO) controllers. This simplifies tuning and mitigates the problems of modeling nonlinear

couplings. The main objective of the base (regulatory) level is to minimize cross-couplings to prevent a chain reaction of actuator oscillations and the complete loss of system functionality. So, we develop a new, advanced control system for the TEP built upon SISO controllers, while mitigating the shortcomings of previously developed decentralized systems by incorporating supplementary functional blocks.



In the figure, P denotes a positive correlation between the controlled variables, N denotes a negative correlation. Correlations with p=1 are shown in bold. Correlations with p<0.7 are not visualized. Dashed lines indicate groups of strongly correlated parameters.

Fig.2. Results of correlation and degree of association analysis.

To achieve this goal, the following tasks must be addressed:

1) develop a control system structure grounded in the physical, dynamic, and economic characteristics of the plant, drawing on the results of recent analyses;

2) minimize undesirable actuator oscillations induced by measurement noise;

3) mitigate the impact of cross-couplings within the process;

4) reconstruct continuous signals from discrete concentration measurements, which inherently complicate control;

5) ensure robust control system performance under significant disturbances, informed by a rigorous disturbance impact analysis;

6) minimize the economic cost function to a reasonable extent without compromising system robustness;

7) investigate methods to eliminate the effects of process and measurement noise, and evaluate how this noise neutralization impacts overall closed-loop performance.

4 DEVELOPMENT OF A NEW TEP CONTROL SYSTEM

4.1 Identifying key parameters, conflicts and risks

Utilizing the findings from the literature review, we identify key parameters and conflicting objectives (trade-offs) within the process. First, it is essential to highlight the following interaction pathways, which are critical for formulating a robust control strategy:

Material balance. The supply of feed streams u_1–u_4 affects the reactor level (y_8) and the reactor inlet flow rate (y_6), which subsequently impacts

the system pressure (y_7) due to vapor/liquid phase shifts.

Composition and discharge streams. The recycle and purge valves (u_5, u_6) alter the component concentrations and vessel levels, which directly affects the reaction regime.

Energy balance. Cooling actions (u_{10}, u_{11}) govern the thermal dynamics (y_{21}, y_{22}, y_9), which, in turn, significantly alter the reaction kinetics within the reactor and indirectly influence the system pressure and product flow rate/composition.

4.2 Strategy for process disturbance rejection

Every realized in the simulation model disturbance upsets the mass and energy balances. In a recycle loop, a change in stoichiometry (IDV1) or the accumulation of inerts (IDV2) alters the gas composition. This requires output adjustment, but a change in product flow upsets the material balance, and increasing the purge rate alone may not be sufficient. An increase in gas inventory threatens to overload the compressor due to rising pressure, so purging is combined with adjusting the reaction rate (via feed flow *A*). Temperature and enthalpy disturbances (IDV3, IDV4) require immediate compensation by cooling; otherwise, a delay or actuator saturation (100% valve opening) will lead to thermal runaway.

The process also loses stability due to:

1) Actuator saturation (reaching 0% or 100% bounds). Actuator saturation effectively breaks the control loop, leading to exponential parameter drift, and the accumulated integral windup severely destabilizes the system during an attempt to recover.

2) Control loop interactions. Temperature compensation efforts can disturb the system pressure, causing resonance. Oscillations are transmitted in a cascade between units, meaning self-oscillating modes must be strictly avoided.

4.3 Operating mode of the process

The optimal steady-state operating mode (Mode 1), derived in [27], is adopted as the baseline.

Variable designations and operating parameters are illustrated in the diagram in Fig. 3.

Mode 1 is primarily driven by economic criteria. Operating costs are a function of the steam flow rate, compressor power consumption (which is driven by the recycle flow rate), the purge flow rate, and the amount of inert gas *B* discarded in the purge. Relative to the nominal base case, the steam flow rate and reactor level are minimized, while the reactor pressure is maximized. In this scenario, the purge flow rate and its composition become the primary economic indicators: compared to the base case, the purge rate is reduced by approximately one-third, and the molar concentration of *B* is increased by roughly two-thirds. Because the system is not initialized at the default base case, the control system is forced to drive the process to this new steady-state operating point immediately upon startup, even in the absence of external disturbances.

4.4 Control system design requirements

The designed control system must satisfy the following criteria: 1) ensure cost-effectiveness by minimizing operating costs; 2) employ rationally justified controller tunings; 3) minimize the detrimental impact of sensor noise and dead times on overall closed-loop performance.

The development of the control system is conducted in two stages. Initially, a baseline control system comprising exclusively P and PI controllers. It was designed to maintain basic process operability. Subsequently, this baseline framework is upgraded into an advanced control system to fulfill the comprehensive overarching objectives.

4.5 Simulation setup

The control system was implemented and evaluated using the MATLAB/Simulink environment alongside the C-based MEX simulator [9].

The entire control architecture operates as a discrete-time system with a uniform sampling interval T_s. This logic is encapsulated within an Atomic Subsystem block In Simulink.

The ode15s solver was utilized for numerical integration due to the stiff nature of the process dynamics.

To ensure the strict reproducibility of the experiments, the random number generator seed was fixed at 12345.

The base sampling interval T_s was determined utilizing the empirical rule of thumb which states that the sampling period should be approximately one-tenth of the smallest time constant within the controlled plant. For the TEP, the flow valve actuators exhibit the fastest dynamics, with time constants *T* ranging from 5 to 9 seconds (i.e., 5/3600 to 9/3600 hours). Consequently, the sampling interval was calculated as follows:

$$T_s = \frac{T_{\min}}{3600\times 10} = \frac{5}{3600\times 10} \approx 1.39\times 10^{-4} \text{ hours} \quad (2)$$

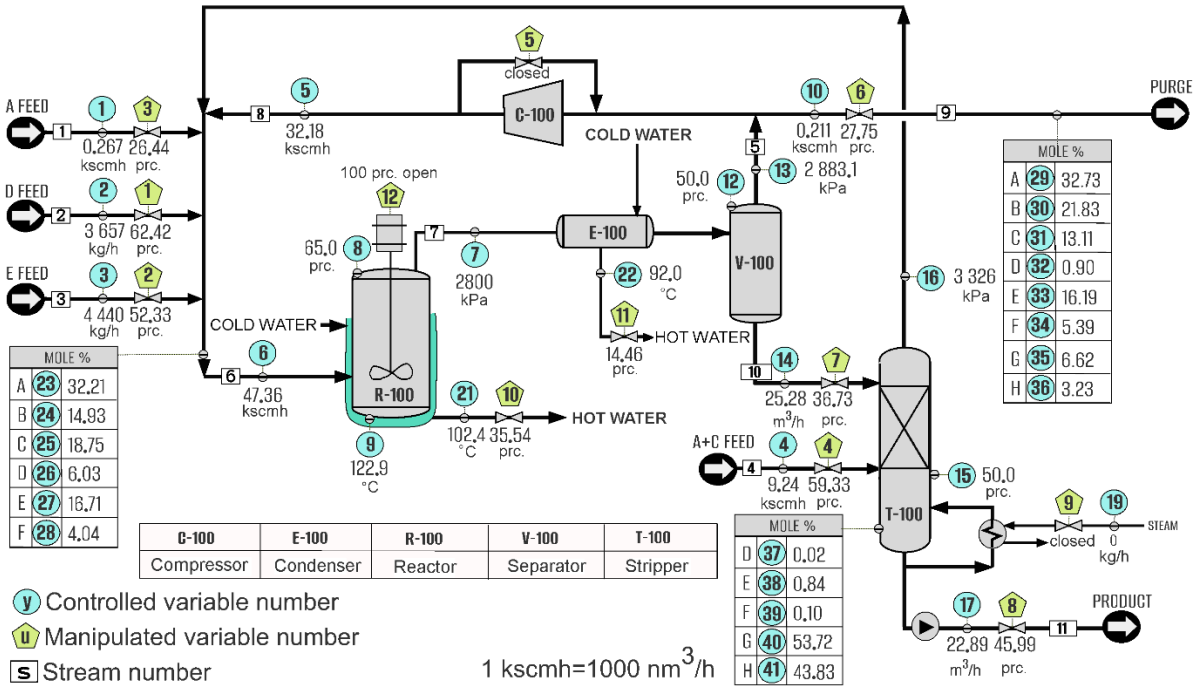


Fig.3. Parameters of the selected operating mode and variable designations.

4.6 Baseline control system design

The primary objective of the baseline control system is to sustain steady-state operation at the nominal throughput in the absence of significant external disturbances.

Initially, all manipulated variables (inputs) are fixed at their nominal steady-state values by applying constant signals: u_{nom} = [62.4160, 52.3280, 26.4403, 59.9328, 0, 26.7475, 36.7264, 45.9852, 0, 35.5439, 14.4569, 100]%. Subsequently, these constant inputs are sequentially replaced by active feedback controllers to systematically close the individual control loops.

4.6.1 Diagram of the baseline control system structure

The structural diagram is shown in Fig. 4.

Key features of the baseline control architecture include the following:

1) Maintaining a constant recycle flow rate is not a primary objective.

2) The purge flow rate is held constant.

3) The purge concentration is regulated via the composition of *C*, which is manipulated by varying the *A*+*C* feed rate into the separator. This indirectly stabilizes the concentration of inert *B* at the reactor inlet.

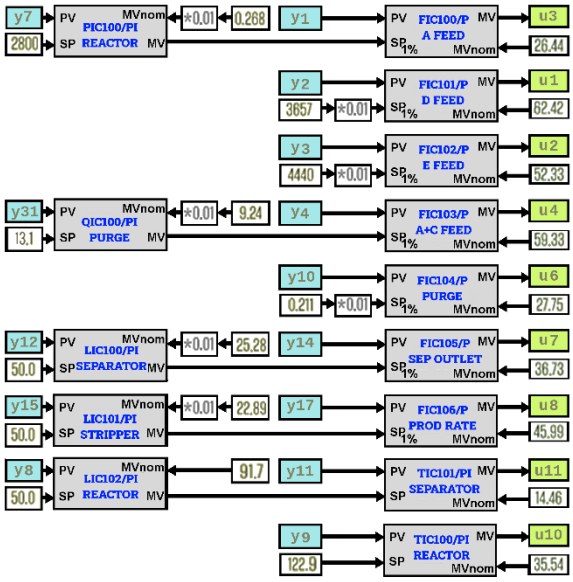


Fig.4. Baseline control system structure.

4) The feed rate of stream *A* to the reactor is indirectly controlled via the reactor pressure, as

pressure serves as an indicator of the reaction rate, and component *A* acts as the primary reaction driver.

5) The feed rates of streams *D* and E are strictly maintained.

6) The reactor temperature is held constant.

7) Liquid levels in the primary vessels are held constant.

The reactor level is controlled using the separator temperature, leveraging the strong dynamic coupling between the system's material balance and the separation temperature.

4.6.2 Controller implementation

For the baseline control system, discrete P and PI controllers are employed, utilizing the standard ISA algorithm form:

$$C(s) = k_p \cdot \left(1 + \frac{1}{T_i \cdot s}\right). \quad (2)$$

The integral term is implemented using the Backward Euler approximation. To prevent integral saturation, a back-calculation anti-windup algorithm with a tracking gain of $1/T_i$ is utilized.

4.6.3 Flow controllers tunings

Flow rates are stabilized using inner (slave) controllers within cascade loops. Seven controllers are implemented for channels characterized by an actuator time constant T_n and a steady-state gain $k = y_n/u_n$. Because T_n is practically negligible, P-controllers are sufficient for flow stabilization. The proportional gain is calculated as $k_p = 0.5k$. To account for potential variations in throughput, the master controller provides a setpoint normalized to 1% of the nominal production rate (denoted as $SP1\% = y_n/100$). The actual setpoint signal passed to the controller is scaled by a factor of 100. The calculated parameters for these flow controllers are summarized in Table 1.

Table 1.

Flow controller parameters

P	FIC102	FIC 100	FIC 101	FIC 103	FIC 104	FIC 105	FIC 106
u #	3	1	2	4	6	7	8
T_n	6	8	8	9	5	5	5
u_n, %	26.44	62.416	52.328	59.933	26.747	36.726	45.985
y #	1	2	3	4	10	14	17
y_n	0.267	3657	4440	9.24	0.211	25.28	22.89
*SP*1%	0.00267	36.57	44.4	0.0924	0.00211	0.2528	0.2289

At this stage, controllers are active for nearly all primary manipulated variables, with only two exceptions. Operating the process in this configuration without external disturbances yields stable conditions for only 0.25 hours. Initially, the controller outputs and process variables fluctuate within a narrow 1% margin; however, the process inevitably destabilizes: the recycle is 51 kscmh, the pressure flow rate rises to 39 kscmh, the reactor feed reaches hits the 3000 kPa emergency shutdown limit, and the reactor temperature plummets to 90 °C.

4.6.4 Temperature in separator controller tuning

For the analytic delayed plant model:

$$P(s) = \frac{-11.18}{0.40107 \cdot s + 1} e^{-1/36 \cdot s} \quad (3)$$

MATLAB's pidtune algorithm yields PI controller parameters: k_p = -0.112 and T_i = 0.174. This results in a closed-loop gain margin of 17.4, which is highly robust. Although this controller successfully halts the rapid divergence of the controlled variable in the isolated nominal model, the plantwide control system ultimately remains unstable.

4.6.5 Reactor temperature controller tuning

Consequently, an operational tolerance of at least ±15-20% must be accommodated, yielding an estimated process gain range of $K \in [-0.55, -0.35]\ ^{\circ}\mathrm{C}/\%$.

Focusing on the median value, the proportional gain is calculated as $k_p = -2/0.45 \approx -4.44$. The actuator time constant is 5 seconds, and there is no dead time in this control channel.

The reactor is an open-loop unstable plant requiring rigorous tuning and a smooth, overdamped response to prevent thermal runaway. The controller's primary task is to decisively stabilize the system before minimizing tracking

error. Because the PI controller's integral component introduces up to a -90° phase lag that can critically delay responses, k_p and T_i must be sufficiently large. This ensures the PI controller behaves like a rapid P-controller at high frequencies.

The actuator time constant T is adopted as the effective dead time, τ_e. For an unstable first-order process with dead time, guided by Skogestad's IMC rules, the integral time is defined as $T_i = \nu \cdot \tau_e$, where ν is an adjustable factor providing a safety margin. This factor must be approximately an order of magnitude greater than τ_e.

The PI controller adds its own phase shift:

$$\phi_{PI}=-90^{\circ}+\arctan(\omega T_i). \quad (4)$$

At the operational cutoff frequency (ω_c), the controller should mimic a pure P-controller to prevent severe phase distortion. Hence, the integral contribution must remain marginal. The phase lag induced by the integrator near the actuator-limited frequency ($\omega \approx 1/\tau_e$) should be minimal (e.g., no more than 5–10 degrees, or roughly 0.1–0.2 radians). Since ω_c is bounded by the actuator to preserve the stability margin $\omega_c \approx 1/(2\tau_e)$, substituting this parameter demonstrates the limits of allowable integral action:

$$\frac{1}{\frac{1}{2\tau_e}\cdot T_i} \approx [0.1.0.2] \rightarrow \frac{2.\tau_e}{T_i} \approx [0.1..0.2]. \quad (5)$$

Given an effective dead time of $\tau_e = 5$ seconds, the integral time T_i is evaluated between 50 and 100 seconds. To incorporate an adequate safety margin, an intermediate value of 75 seconds is selected. Crucially, to maintain consistency with the simulation framework, this is integrated as exactly 75/3600 astronomical hours.

Simulating with these controllers maintains target temperatures for approximately 3.5 hours. However, latent plantwide instability emerges as the recycle flow and reactor level decline. Simultaneously, the separator liquid level reaches 100% capacity, threatening the stripper. Consequently, explicitly stabilizing vessel levels becomes mandatory.

4.6.6 Separator and stripper level controller tuning

Having stabilized the process energy balance (temperature), the material balance (vessel levels) must subsequently be stabilized. Because the outlets of the separator and stripper are governed by pumps and control valves, these channels exhibit integrating dynamics (i.e., they act as integrating elements)

Consider the FIC105 controller, which is configured as the inner (slave) loop for the separator level controller. At a nominal setpoint of $SP1\% = 0.2528$, the level rises rapidly. Empirical testing establishes that the level stabilizes when $SP1\%$ is scaled by a factor of 1.17. The rate of change for the nominal SP1% case is estimated as follows:

$$\Delta S=0-57.75=-57.75\%/\text{hour}, \quad (5)$$
$$\Delta u=r\cdot 1.17-r=0.043.$$

In general, the process is described by an integrating element:

$$P(s) = \frac{K_L}{s} \quad (6)$$

The process gain K_L is calculated as $K_L = (1/0.043)\cdot 57.7 \approx 1341.86$.

To ensure smooth operation without overshoot, the controller is tuned using pole placement for an overdamped response. The liquid level is strictly constrained within 30–70%. To prevent actuator saturation and nonlinearities, the initial control surge at maximum error must not exceed the allowable control input deviation (the slave controller's nominal setpoint). Consequently, a proportional gain of $k_p = 0.012$ is selected.

To further ensure smoothness, oscillatory behavior must be strictly avoided. A closed loop comprising an integrating plant and a PI controller yields a second-order characteristic equation:

$$s^2 + (K_L \cdot k_p)s + \frac{K_L \cdot k_p}{T_i} = 0 \quad (7)$$

To achieve a smooth, non-oscillatory response, the damping ratio ζ must be ≥1. An overdamped design is chosen, setting ζ=1.5. The integral time is then calculated as follows:

$$T_i = \frac{4\cdot\zeta^2}{K_L k_p} = \frac{4\cdot 2.25}{K_L \cdot k_p} = \frac{9}{K_L \cdot k_p} = \frac{9}{16.1} \approx 0.56 \text{ hour}$$

Integrating the LIC100 master controller with these settings (utilizing a negative k_p due to the reverse-acting nature of the loop) successfully stabilizes the separator level in less than an hour.

The LIC101 master controller, cascading to FIC106 for stripper level control, is configured using an identical methodology. Directing the slave controller to $SP1\% = 0.2289$ results in a rapid level increase. In this instance, scaling the

setpoint by a factor of 1.2 stabilizes the stripper level. Consequently

ΔS=0-125.78=-125.78%/hour

Δu=r·1.2-r=0.0458Δ

Let's calculate the object's gain

Limitations

$$K_p \le \frac{u_{max}}{e_{max}} = \frac{0.22898}{20} = 0.0114$$

Calculating the process gain

$$K_L = \frac{1}{0.0458} \cdot 125.78 \approx 2746.29$$

and applying the same operational constraints

$$k_p \le \frac{u_{max}}{e_{max}} = \frac{0.22898}{20} = 0.0114$$

yields a proportional gain selection of k_p = 0.011. The corresponding integral time is:

T_i=931.43≈0.29 hour.

Connecting the LIC101 master controller with these tuning parameters (negative k_p) achieves rapid level stabilization. At this juncture, both primary vessel levels are stabilized by their respective cascade loops. However, the overall process remains susceptible to pressure imbalances and ultimately begins to diverge after approximately 4.5 hours of operation.

4.6.7 Tuning rest of controllers

First, the QIC100 master controller is implemented. The empirical transfer function for this channel is derived as:

$$P(s) = \frac{5786s^2 + 1.61 \cdot 10^4 s + 8909}{29.74s^3 + 26.05s^2 + 14.16s + 1} \quad (8)$$

The controller is tuned for a fast dynamic response, yielding parameters k_p = 0.00146 and T_i = 4.26. Under these conditions, the influx of component *B* into the reactor stabilizes, while the reactor pressure and level drift smoothly downward until the 5th hour, followed by a sharper upward trajectory.

Subsequently, the LIC102 master controller is implemented. An empirical transfer function is obtained, yielding an integrating process with dead time: $(1/1.2s)\cdot e^{-0.12s}$. The pidtune program calculated PI-controller with k_p = 2.9, T_i = 1.75.

Finally, the PIC100 master controller is configured. Based on the empirical transfer function derived for this specific control channel:

$$P(s) = \frac{-3.138 \cdot 10^6 s^3 - 5.411 \cdot 10^5 \cdot s^2 - 2.172 \cdot 10^6 s - 1.129 \cdot 10^1}{162.6.8^4 + 51.42.8^3 + 220.7s^2 + 18.45 \cdot 10^{16}}$$

the pidtune algorithm yields the following PI controller tunings:

k_p = -1.21e-05, T_i = 6.18.

4.6.8 Baseline control system evaluation

While maintaining steady-state operation under nominal conditions, the baseline system exhibits critical shortcomings:

1) Oscillatory control signals. Non-temperature sensor noise compounds in cascade loops, causing excessive actuator movement despite process inertia.

2) High noise variance. Significant noise in flow, level, and concentration sensors causes sharp setpoint jumps, requiring filters more sophisticated than standard low-pass designs.

3) Unrejected concentration disturbances. The discrete nature and dead times of concentration sensors make simple static feedforward compensation unacceptably aggressive for flow controllers.

4) Synchronous vessel oscillations: These oscillations drive undesirable fluctuations in the overall plant production rate

4.7 Design of an advanced control system

4.7.1 Advanced control system structure

Key algorithmic and functional enhancements to the control elements include:

1) Inner (slave) flow loops employ controllers embedded with internal actuator models.

2) Second-order discrete filters are applied to the setpoints transmitted from the master controllers to the slave controllers.

3) Discrete concentration measurements are reconstructed into continuous signals utilizing a discrete Kalman Filter (KF) based on a Constant Velocity (CV) model.

4) Production rate fluctuations are attenuated by implementing a feedforward compensator based on the input disturbance.

5)The product concentration is regulated via a PI controller augmented with a modified Smith predictor scheme to enhance robustness against dead time.

6) The purge flow is regulated by a PI controller that incorporates control action smoothing near its operational limits, thereby mitigating nonlinear effects that could induce system instability.

Key architectural features of the control strategy include:

1) Maintaining a strict stoichiometric *A/C* ratio at the reactor inlet.

2) System pressure is regulated by cooperatively adjusting the purge flow rate and

modulating the overall throughput within a ±20% range of its nominal value.

3) Process throughput is primarily throttled by minimizing the feed of reactant *E* to strictly required levels, thereby preventing unnecessary increases in operating costs.

4) The concentration of inert *B* in the purge stream is indirectly stabilized by controlling the concentration of the adjacent light component, *C*, which is achieved by manipulating the combined *A+C* feed rate.

4.7.2 Flow measurement filtering

TEP flow sensors often exhibit unphysical transient spikes. Traditional low-pass filters introduce significant phase lag, while cascade loops offer limited noise attenuation. To resolve this, a discrete Kalman Filter (KF) is implemented. Because flow channels behave predictably as first-order lags, this mathematical model is converted into a discrete-time state-space representation within the KF to neutralize white noise:

$$x_{k+1} = e^{-T_s/T} x_k + k\left(1 - e^{-T_s/T}\right)u_k, y_k = x_k \qquad (9)$$

The measurement noise covariance scalar, *R*, is related to the difference in orders of magnitude (base 10) between the control signal and the measurement. It is calculated using the following empirical formula:

$$v = 10^{1.5.(\log 10(y_{nom}) - 1og10(u_{nom}))+6)} \qquad (10)$$

By extracting the mantissa *M* and exponent *E* from variable *v* the value of *R* is determined, while the process noise covariance *Q* is strictly set to 1.

To demonstrate this, consider the FIC102 controller operating under a constant setpoint. Introducing the KF into the measurement channel with $R = 1.0148 \times 10^3$ yields virtually perfect signal smoothing. Similar high-quality results are observed under dynamic reference tracking.

4.7.3 Introduction of setpoint filters in cascade loops

In cascade systems, transmitting setpoints from the master to the slave controller is complicated by extreme noise in TEP level and recycle sensors. This makes internal model filtering unfeasible, while FIR filters require an excessive number of states. A more rational approach is filtering the master controller's output rather than raw measurements. Thus, the transmitted setpoint is processed through a second-order discrete filter (S2F), derived via bilinear transform, yielding this transfer function:

$$H(z) = \frac{b_0 + b_1 z^{-1} + b_2 z^{-2}}{1 + a_1 z^{-1} + a_2 z^{-2}}, \qquad (11)$$

Ultimately, the integration of the discrete KF reduces the Integral Square Error (ISE) and Integral Absolute Error (IAE) performance indices across all flow controllers by one to three orders of magnitude, crucially without introducing any phase delay into the control loop.

where the coefficients b_i and a_i depend on the filter type (low-pass), the natural cutoff frequency f_n, the damping ratio $\zeta = 0.707$ (which corresponds to a maximally flat amplitude response in the passband, characteristic of a Butterworth filter), and the discrete sampling step Δt.

A cutoff frequency of $f_n = 10$ units/hour was selected, defining the point at which the signal amplitude is attenuated by -3 dB.

Consider the combined contribution of the Kalman filter and the S2F to the closed-loop performance during disturbance rejection. The transient responses in Fig. 7 illustrate the dynamics of the LIC100-FIC105 cascade, specifically showing: the raw level measurement, the unfiltered calculated setpoint of the master controller, the filtered setpoint received by the slave controller (via S2F), and the filtered control action of the slave controller (via KF). Filtered signals are highlighted in green.

An analysis of the setpoint filtering performance yielded the following quantitative metrics:

1) Signal-to-Noise Ratio (SNR): 31.7 dB. The noise power accounts for only ~0.07% of the original signal's power, indicating highly effective noise suppression.

2) Variance reduction: 59.5%. The filter successfully eliminated nearly 60% of the raw signal's variability while fully preserving the primary process dynamics.

3) Attenuation in the stopband (>3 cycles/hour): 52.7 dB. High-frequency components are attenuated by a factor of over 300 in amplitude, confirming the filter's capability to eliminate rapid, aggressive fluctuations.

4) Phase lag: there is virtually no time delay between the input and filtered signals. This negligible phase shift ensures the filter is highly suitable for real-time, closed-loop control applications.

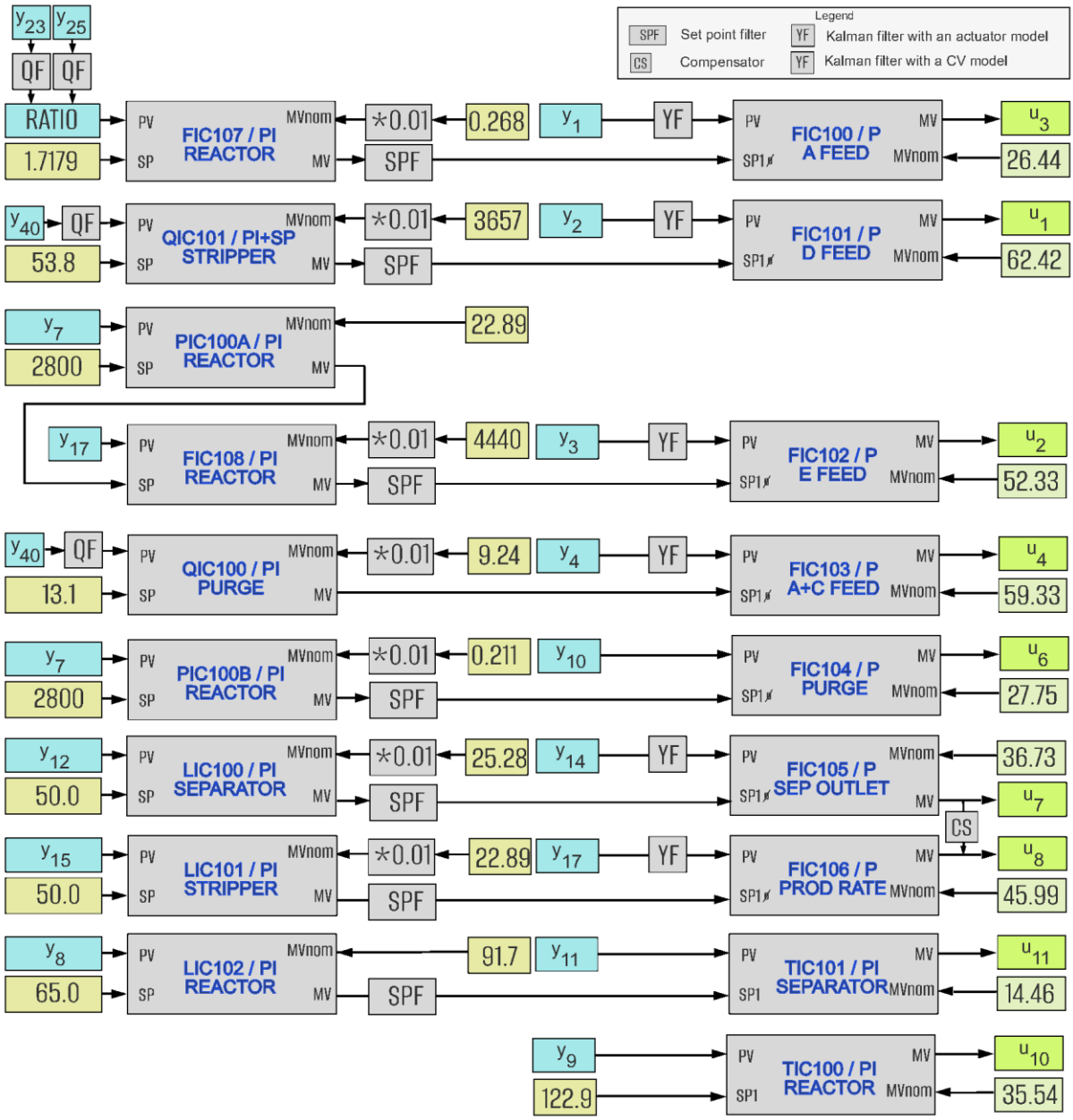


Fig.5. Transient responses of the LIC100-FIC105 cascade under various filtering configurations.

Consequently, integrating these two filtering techniques is sufficient to ensure stable control while completely suppressing unwanted high-frequency oscillations in the manipulated variables. The LIC101-FIC106 cascade is upgraded utilizing an identical methodology. For the LIC102-TIC101 cascade, implementing the setpoint filter on the TIC101 alone is sufficient.

4.7.4 Attenuating production rate fluctuations

The product flow rate is primarily governed by the liquid level in the stripper. For the stripper, any variation in the separator level acts as a direct upstream disturbance. Provided that the combined *A+C* feed rate remains constant, this disturbance can be effectively neutralized by implementing a feedforward compensator.

To achieve this, the control output from the slave controller FIC105 is scaled by the ratio of the nominal setpoints of controllers FIC106 and FIC105 (i.e., 45.985 / 36.726). The baseline feedback control signal generated by FIC106 is then dynamically augmented with this scaled feedforward term derived from FIC105. Simultaneously, a unit delay (one discrete sampling step) is incorporated into the FIC106

control calculation to properly synchronize the dynamic response.

4.7.5 Filtering of concentration measurements

Process analyzers measure the component concentrations in streams 6 (reactor inlet), 9 (purge), and 11 (product). However, these measurements present significant control challenges. The analyzers for streams 6 and 9 operate with a discrete sampling interval of 0.1 hours and an equivalent dead time.

The product concentration analyzer (stream 11) operates with a sampling interval of 0.2 hours and a corresponding 0.25-hour dead time. Furthermore, these discrete signals are heavily contaminated with measurement noise and exhibit sharp transient spikes, which are highly detrimental to smooth control action.

To ensure signal smoothness and attenuate these peaks, a discrete Kalman Filter (KF) utilizing a kinematic Constant Velocity (CV) model is employed. The state variable (position x) updates according to the kinematic equation:

$$x_{k+1} = x_k + v \cdot \Delta t \qquad (12),$$

where velocity v is assumed constant between sampling instants.

Unlike a standard low-pass filter, which would simply stagnate at the constant discrete value between samples (exhibiting a zero-order hold effect), the CV-based KF extrapolates the trajectory based on the estimated velocity.

This dynamic "inertia" effectively smooths the discrete staircase steps into continuous, sloping transitions. The state vector takes the form $x_k = [x_i \quad v_i]^T$.

The system dynamics is described by the following state-space model:

$$\begin{aligned} x_{k+1} &= A \cdot x_k + w_k, \\ y_k &= C \cdot x_k + v_k, \end{aligned} \qquad (13)$$

where w_k is the process noise vector, v_k is the measurement noise vector.

Standard CV model is

$$A = \begin{bmatrix} 1 & \Delta t \\ 0 & 1 \end{bmatrix}; C = [1 \ 0]; B = D = 0. \qquad (14)$$

For the reconstruction of the component A concentration signal at the reactor inlet, the filter tuning matrices were determined empirically. For sensors with a 0.1-hour dead time, the covariance matrices were set to $R = 1$, $Q = \mathrm{q} \times 10^{-7} \times I$, and for the sensor with a delay of 0.25 (product concentration) as R = 1, $Q = q \times 10^{-5} \times I$.

The resulting filtered signal provides a smooth, continuous trajectory that is significantly more suitable for closed-loop control than the raw discrete measurements.

4.7.6 Control of *A*/*C* ratio in the reactor feed

According to the optimal steady-state operating mode derived in [27], the target molar concentrations for components A and C are established at 32.21% and 18.75%, respectively. To maintain this stoichiometric balance, the FIC107 master PI controller is implemented, utilizing the dynamically measured concentrations of these specific components. The empirically determined PI tuning parameters for this loop are k_p=0.02, T_i=5.

4.7.7 Product *G* concentration control

The empirical transfer function for this channel is derived as:

$$P(s) = \frac{0.4232 \cdot s + 0.1718}{2.492 \cdot s^2 + 1.72 \cdot s + 1} \cdot e^{-s} \qquad (15)$$

Because the dead time is strictly constant, a Smith predictor structure is ideally suited for this control loop. This architecture proactively compensates for the 1-hour dead time based on the internal process model. To enhance system robustness, a low-pass filter with a time constant of $T = 0.1$ is incorporated into the prediction loop, adhering to the methodology proposed in [35]. Utilizing MATLAB's pidtune algorithm and targeting a 90° phase margin (PM), the PI controller parameters are calculated: $k_p = 9.76 \times 10^{-5}$, $T_i = 6.94 \times 10^{-5}$.

4.7.8 Production rate control

The empirical transfer function for this control channel is derived as:

$$P(s) = \frac{-0.1477 \cdot s + 0.3851}{0.7476 \cdot s^2 + 1.92 \cdot s + 1} \cdot e^{-0.00996s} \qquad (16)$$

The corresponding PI controller tuning parameters are determined as k_p=2.94 and T_i=1.75.

4.7.9 Reactor pressure control

Because the process operates near the maximum allowable pressure limit, maintaining

this parameter is strictly critical. During severe transient events, such as disturbances IDV1 and IDV2, reactor pressure becomes the most vulnerable system variable. While stabilizing the stoichiometric A/C ratio generally mitigates sharp pressure spikes induced by compositional shifts, it does not completely guarantee their prevention.

Counteracting pressure surges via traditional purge flow modulation is often insufficient during extreme transients and incurs economic penalties. The proposed architecture introduces a supplementary mechanism: concurrently increasing the reactant E feed. While risking reactant E loss, this rapidly arrests dangerous pressure surges, ensuring process safety.

5 CONTROL SYSTEM EXAMINATION

The proposed control system is evaluated by applying typical setpoint changes and external disturbances to the process model.

The time-domain results demonstrate that incorporating advanced filtering into the control architecture significantly improves overall control performance, enhances the stabilization of process variables, and leads to the almost complete suppression of actuator high-frequency chattering. This consistent improvement is observed across the majority of the evaluated disturbance scenarios. For cases where the economic benefit is most pronounced, the comparative simulation results are summarized in Table 2.

Table 2.

Average production cost during transient simulations under typical model disturbances

IDV	Noise-free baseline simulation	Unfiltered baseline system	Proposed advanced system
1	126.99	127.04	123.9
2	118.82	119.05	118.33
3	124.11	124.18	122.12
4	122.57	122.63	120.38
8	127.48	127.50	124.52
9	124.16	124.22	122.17
10	124.40	124.48	122.42
11	123.90	123.96	121.93
12	121.14	121.32	120.81
13	120.04	120.19	119.35
14	124.15	124.23	122.19

The tuning parameters for the pressure controllers were determined empirically. Controller PIC100A is configured as a proportional (P) controller with $k_p = 1 \times 10^{-3}$. Controller PIC100B is configured as a PI controller with tunings $k_p = -3.7154 \times 10^{-4}$ and $T_i = 26.995$.

This approach successfully eliminates severe sensor noise effects without compromising dynamic tracking. Compared to unfiltered systems, it improves control metrics, minimizes economic costs, and stabilizes overall production across various disturbances.

CONCLUSIONS

This study addresses the challenge of designing an automatic control system for complex, open-loop unstable processes, utilizing the Tennessee Eastman Process (TEP) benchmark to explicitly account for the operational characteristics of industrial measuring equipment and actuators. Inherently, measurement noise and discrete sampling in such environments induce severe actuator oscillations, which degrade control reliability and significantly shorten equipment lifespan. In classical control solutions, this problem has largely been neglected due to the detrimental phase lag that standard low-pass filters impose on system stability margins.

The primary contribution of this research is the development of a novel, hierarchical multi-loop control architecture. Within this framework, decentralized PI controllers are augmented with advanced filtering and predictive techniques, specifically: discrete Kalman filters (including kinematic Constant Velocity models for discrete concentration measurements), second-order setpoint filters within cascade loops, and Smith predictors for dead-time compensation.

The implementation of the proposed approach yielded the following key outcomes:

1. Near-complete suppression of high-frequency sensor noise (across level, flow, and concentration measurements) without introducing critical phase lag into the control loops.
2. Elimination of excessive chattering in control valves and pumps, thereby drastically reducing mechanical wear.
3. Effective mitigation of cross-coupling interactions and smooth rejection of typical process disturbances without compromising overall dynamic performance.
4. Enhanced economic efficiency (evidenced by a reduction in average production costs) achieved by maintaining the plant more rigorously at its optimal steady-state operating point.

This approach successfully secures the required control quality while avoiding the "black-box" limitations inherent in large-scale Multivariable Predictive Control (MPC) systems, ensuring practical applicability and transparency in industrial settings.

References

[1] Lyman P. R., Georgakis C. Plant-wide control of the Tennessee Eastman problem. *Comput. Chem. Eng.*, 1995, vol. 19, no. 3, pp. 321-331. https://doi.org.10.1016/0098-1354(94)00057-u

[2] Mustafa F., Ahmed I., Basit A., Alqahtani M., Khalid M. An adaptive metaheuristic optimization approach for Tennessee Eastman process for an industrial fault tolerant control system. *PLOS ONE*, 2024, vol. 19, no. 2, p.e0296471. https://doi.org.10.1371/journal.pone.0296471

[3] Hartung, F., Franks, B. J., Michels, T., Wagner, D., Liznerski, P., Reithermann, S., Fellenz, S., Jirasek, F., Rudolph, M., Neider, D., Leitte, H., Song, C., Kloepper, B., Mandt, S., Bortz, M., Burger, J., Hasse, H., Kloft, M. Deep Anomaly Detection on Tennessee Eastman Process Data. *Chem. Ing. Tech*, 2023, vol. 95, no. 7, pp.1077-1082. https://doi.org.10.1002/cite.202200238

[4] McAvoy T. J., Ye N. Base control for the Tennessee Eastman problem. *Comput. Chem. Eng.*, 1994, vol. 18, no 5. pp. 383–413. https://doi.org.10.1016/0098-1354(94)88019-0

[5] Juliani Correa de Godoy R., Garcia C. Plantwide Control: A Review of Design Techniques, Benchmarks, and Challenges. *Industrial & Engineering Chemistry Research*, 2017, vol. 56, no.8., pp. 7877-7887 https://doi.org.10.1021/acs.iecr.7b00416 .

[6] Downs J.J., Vogel E.F. A plant-wide industrial process control problem. *Computers & Chemical Engineering*, 1993, vol. 17, no. 3, pp. 245–255. https://doi.org.10.1016/0098-1354(93)80018-i.8

[7] Sales-Cruz M., Cameron I., Gani R. Tennessee Eastman Plant-wide Industrial Process Challenge Problem. In Product and Process Modelling, 2011, vol. 7, Elsevier U.K., pp. 273-303

[8] Russell E. L., Chiang L. H., Braatz R. D. Tennessee Eastman Process Fortran Codes and Data. https://github.com/camaramm/tennessee-eastman-profBraatz, 2017.

[9] Bathelt A., Ricker N. L., Jelali M. Revision of the Tennessee Eastman Process Model. *9th IFAC Symposium on Advanced Control of Chemical Processes (ADCHEM 2015)*, 2015. pp. 101–106. https://doi.org.10.1016/j.ifacol.2015.08.199

[10] Vosloo J., Uren K. R., Van Schoor G., A complete and open Simulink model of the Tennessee Eastman process (COSTEP). *SoftwareX*, 2025, vol. 31, p. 102217. https://doi.org.10.1016/j.softx.2025.102217 .

[11] Yapur S. F. Controlled-Variable Selection based on Chaos Theory for the Tennessee Eastman Plant. *ArXiv Prepr*., 2021.

[12] Yapur S. F. Diseño de un-Sistema de Control para una Planta Completa usando Con-troladores Fraccionales. Universidad Nacional del Litoral, 2021.

[13] Yapur S. F. Features of linear models that may compromise model-based, plant-wide control techniques. The case of the Tennessee Eastman plant. *ArXiv Prepr*, 2022.

[14] Prabir K. S., Yi C. Control structure selection for open-loop unstable plant with pure in-tegrators using multi-projected systems. *Proceedings of the European Control Conference (ECC),* 2003, vol.37, pp. 1393-1398. https://doi.org.10.23919/ECC.2003.7085156

[15] Luyben W. L., Tyreus B. D., Luyben G. E. Plantwide Process Control. New York, McGraw-Hill, 1998.

[16] Seborg D., Edgar T., Mellicamp D., Doyle F. Process Dynamics and Control. 4th ed. Hoboken, (N.J.), Wiley, 2020.

[17] Marlin T. E. Process Control: Designing Processes and Control Systems for Dynamic Performance. 2nd ed. New York, McGraw-Hill, 2000.

[18] Implementation of Luyben's Plantwide Control Structure for the Tennessee Eastman Process (2021). URL: https://gitlab.com/eastman_tennessee/luyben,

[19] Khatami A., Fatoorehchi Hooman M., Miandoab E. Robust decentralized sliding mode control for the Tennessee-Eastman Process: a plant-wide approach. *Chemical Product and Process Modeling*, 2025, vol.21, no.2, pp. 217–233. https://doi.org.10.1515/cppm-2025-0029 .

[20] Skogestad Sigurd. Plantwide control: the search for the self-optimizing control structure. *Journal of Process Control*, 2000, vol.10, no.5, pp. 487–507. https://doi.org.10.1016/s0959-1524(00)00023-8

[21] Larsson T., Hestetun K., Hovland E., Skogestad S.. Self-Optimizing Control of a Large-Scale Plant: The Tennessee Eastman Process. *Industrial & Engineering Chemistry Research*, 2001, vol. 40, no. 22, pp. 4889–4901, https://doi.org.10.1021/ie000586y

[22] Ye L., Cao Y., Skogestad S. Global Self-Optimizing Control for Uncertain Constrained Process Systems. *IFAC-Pap*, 2017, vol.50, no. 1, pp.4672–4677. https://doi.org.10.1016/j.ifacol.2017.08.691

[23] Jha A., Okorafor O. C. Optimal Plantwide Process Control Applied to the Tennessee Eastman Problem. *Ind. Amp Eng. Chem. Res.*, 2013, vol. 53, no. 2. pp. 738–751 https://doi.org.10.5772/intechopen.76069

[24] Antelo L., Otero-Muras I., Banga J., Alonso A. A systematic approach to plant-wide control based

on thermodynamics. *Computer Aided Chemical Engineering*, 2005, vol. 20, pp. 1105-1110. https://doi.org.10.1016/S1570-7946(05)80026-4

[25] Antelo L., Otero-Muras I., Banga J., Alonso A. A thermodynamic based plant-wide control design procedure of the Tennessee Eastman process. *Computer Aided Chemical Engineering*, 2006, vol. 21, pp. 1413-1418. https://doi.org.10.1016/S1570-7946(06)80245-2

[26] Antelo L., Excler O., Banga J., Alonso A. Robust decentralized control for flexible plant operation: conceptual design and optimal tuning. *Chemical Engineering Transactions*, 2007, vol. 12, pp. 371-377.

[27] Ricker N. L. Optimal steady-state operation of the Tennessee Eastman challenge process. *Comput. Chem. Eng*., 1995, vol. 19, no. 9. pp. 949–959. https://doi.org.10.1016/0098-1354(94)00043-N

[28] Ricker N. L., Lee J. H. Nonlinear modeling and state estimation for the Tennessee Eastman challenge process. *Comput. Chem. Eng*., 1995., vol. 19, no 9. pp. 983–1005. https://doi.org.10.1016/0098-1354(94)00113-3

[29] Ricker N. L. Decentralized control of the Tennessee Eastman Challenge Process. *J. Process Control*. Elsevier, 1996, vol. 6, no. 4. pp. 205–221. https://doi.org.10.1016/0959-1524(96)00031-5

[30] Ye L., Cao Y., Yuan X., Song Z.. Retrofit self-optimizing control of Tennessee Eastman process. *Proceedings IEEE In-ternational Conference on Industrial Technology (ICIT)*, 2016, pp. 866–871. https://doi.org.10.1109/ICIT.2016.7474865

[31] Lebukan D. E. P., Wardana A. N. I., Effendy N. Implementation of Plant-Wide PI-Fuzzy Controller in Tennessee Eastman Process. *IEEE International Seminar on Application for Technology of Information and Communication (iSemantic)*, 2019. pp. 450–454. https://doi.org.10.1109/ISEMANTIC.2019.8884301

[32] Siemens. Configuration of the MPC10x10 for Tennessee Eastman Benchmark Process: Application Example Entry ID: 101978659. Siemens Industry Online Support, 2024. URL: https://cache.industry.siemens.com/dl/files/659/101978659/att_1308230/v1/101978659_pcs7_mpc10x10_en_V11.pdf

[33] Zakharov A. V., Bosman H. S., Jämsä-Jounela S.-L. Two-Phase Model Predictive Control and Its Application to the Tennessee Eastman Process. *Ind. Eng. Chem. Res*, 2013, vol. 52, no 36. pp. 12937–12949. https://doi.org.10.1021/ie401294r

[34] Luo X., Liu Y., Xu F. Interaction Analysis and Decomposition Principle for Control Structure Design of Large-scale Systems. *Chin. J. Chem. Eng*., 2014. vol. 22, no. 1. pp. 59–71. https://doi.org.10.1016/S1004-9541(14)60002-1

[35] Huang H., Chen C., Chao Y., Chen. P. A modified Smith predictor with an approximate inverse of dead time. *AlCHe Journal*, 1990, vol. 36, no.7, pp.1025-1031. https://doi.org.10.1002/aic.690360708

About authors.



Stopakevych Andrii
PhD, Associate Professor. Odesa Polytechnic National University. Area of scientific interests: complex systems. E-mail:stopakevich@gmail.com
ORCID: 0000-0003-1719-9071



Stopakevych Oleksii
PhD, Associate Professor, Senior Scientist.
Area of scientific interests: system analysis and theory of complex control systems, E-mail:stopakevich@op.edu.ua ORCID: 0000-0002-8318-6853